ANALYSIS AND DESIGN OF SUBWAVELENGTH DIFFRACTIVE OPTICAL ELEMENTS FOR POLARIZATION-DIFFERENCE IMAGING

Yale S. Chang (Electrical Engineering)—University of Pennsylvania
NSF Summer Undergraduate Fellowship in Sensor Technologies
Advisors: Dr. Nader Engheta, University of Pennsylvania
Dr. Dennis Prather, University of Delaware

ABSTRACT

Polarization-difference imaging (PDI) has been proven to significantly enhance the detection of targets and their surface features in scattering media. We are currently building a portable prototype PDI camera that can capture a scene at orthogonal linear polarizations and can produce PD images in real time. This paper details the design and analysis of subwavelength diffractive optical elements (DOEs) that will function as linear polarization analyzers in the PDI camera. Using Matlab software, we derived pulse-width modulated subwavelength features from continuous phase functions and modeled the wave propagation through the components using the finite-difference time-domain (FDTD) method. Various lenses operating at incremental wavelengths of the visible spectrum were designed, analyzed, and evaluated. DOEs designed for 400, 450, and 500 nm incident waves performed the most desirably; their intensity ratios, obtained by dividing the focal plane's maximum electric field intensity from TM wave illumination by that from TE wave illumination, remained relatively constant at approximately 2.5:1.

1. INTRODUCTION

1.1 Polarization-Difference Imaging

1.1.1. Biological Basis

Human vision can become severely impaired in obscuring weather conditions such as rain, fog, and snow. The degradation in visual perception is the result of light scattering caused by small particles and the eyes' inability to extract images under veiling light. However, many animal species are naturally adept at navigating through densely scattering media by gift of their sophisticated visual systems. For example, evolution has selectively equipped the green sunfish (*Lepomis cyanellus*) with paired photoreceptors arranged as a square array of double cones [1]. It is hypothesized that the double cones function as birefringent waveguides and linear polarizers, allowing the sunfish to separate orthogonal linear polarizations of light and subsequently subtract these signals to output a polarization-difference image. This biological imaging technique is the inspiration behind artificial polarization-difference imaging (PDI) systems, which have been shown to greatly enhance image quality and target detection in optically scattering media.

1.1.2. Light and Polarization

Light is a transverse electromagnetic (TEM) wave, meaning that its electric and magnetic field vectors are perpendicular both to each other and to the direction of propagation. For a uniform plane wave such as light, its electric field vector can be separated into two linear components that oscillate independently at right angles to each another. Light's state of polarization refers to the orientation and behavior of the resultant electric field vector. More specifically, polarization is defined by the path traveled by the tip of the electric field vector as the light wave propagates through space.

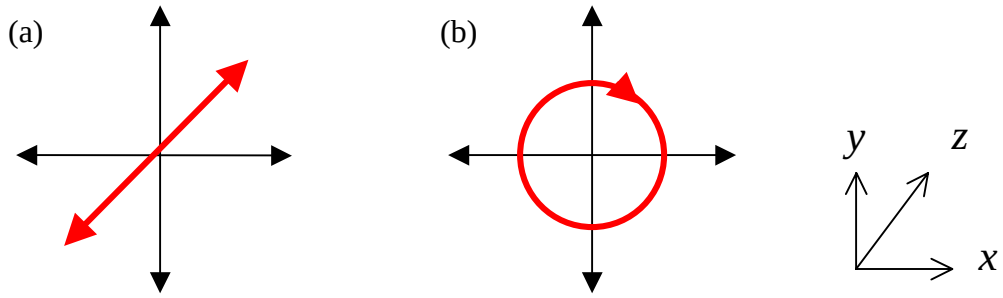

Figure 1.1. A light wave exhibiting (a) linear polarization and (b) circular polarization.

For example, a light wave moving in the *z* direction is linearly polarized if it has only one electric field component (E_x or E_y) or if the two components are in phase [6]. If viewed in the plane perpendicular to the direction of propagation, the tip of the resultant electric field vector will oscillate in time along a straight line (Figure 1.1a).

A light wave is circularly polarized when its two orthogonal electric field components are out of phase by 90° but have equal amplitudes. In this case, the tip of the resultant electric field vector traces a fixed circle when viewed in the plane perpendicular to the direction of propagation (Figure 1.1b). In effect, the tip of the electric field describes a helix in space as time progresses [6].

A linear polarization analyzer is a material or device that confines the vibration of the incoming wave's electric field to planes parallel with its optical axis. Figure 1.2 demonstrates an example of crossed polarization, where two linear polarizers positioned orthogonally are placed in the path of an arbitrarily polarized light beam. The first polarizer transmits only the horizontal electric field component and, as a result, no light passes through the second polarizer, which has a vertical polarization axis.

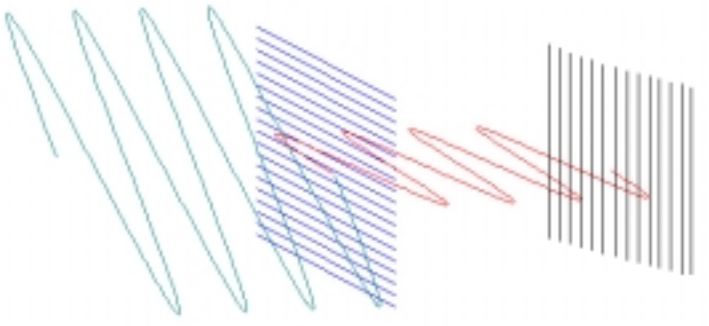

Figure 1.2. Crossed polarizers completely block out an incident light wave.

1.1.3. Concept of Polarization-Difference Imaging

While white light from incandescent sources is initially unpolarized, almost all naturally occurring light is partially linearly polarized after scattering from objects [3]. When the human eye views polarized light, it can sense only color and brightness, which is associated with the sum of all linear polarization components. The eye cannot, however, effectively distinguish the relative magnitudes of the polarized components or the shape of polarization. In essence, the human eye is an example of a conventional imaging system, which is polarization-blind. However, light's state of polarization can convey additional physical details about an imaged scene than intensity alone.

A PDI system, in contrast, extracts polarization information by decomposing an image into two orthogonal linear polarizations, computing their difference signals pixel by pixel, and scaling the difference image for display [2]. Studies by J. S. Tyo, M. P. Rowe, E. N. Pugh, Jr., and N. Engheta of the University of Pennsylvania have demonstrated that PDI systems can produce distinctly visible surface features that are invisible under conventional, polarization-sum imaging (Figure 1.3).

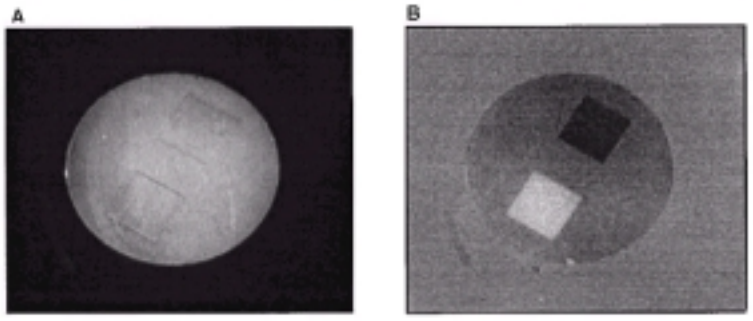

Figure 1.3. An aluminum disk is placed in a tank of water diluted with milk. The patches are not visible under (A) conventional imaging but are discernible using (B) polarization-difference imaging.[2]

The ability of PDI to improve target detection in scattering media arises from its common-mode rejection/differential-mode amplification feature. This feature is a signal-processing technique that allows the extraction of small signals in the presence of other larger signals, provided that their spatial frequency content is different [3]. Common mode rejection proves especially effective in scattering media, where light reflected from a target can travel different paths before reaching the detector. Image-forming light, which reflects back directly from the target to the detector without scattering, is mostly polarized. On the other hand, background light and veiling light—the light scattered into the detector by small particles—are generally unpolarized or may have different polarization. By subtracting orthogonal linearly polarized images, a PDI system rejects the intensity common to both signals, allowing the removal of background and veiling light along with unwanted variations. Amplification of the remaining image-forming light will then magnify small intensity variations created by surface features and improve their visibility [3].

1.1.4. Effectiveness and Applications of Polarization-Difference Imaging

The PDI system discussed above has produced experimental results that validate its robustness. Tyo, Rowe, Pugh and Engheta have shown that PDI is highly sensitive to small signals, where surface features producing an observed degree of linear polarization (ODLP) of less than 1% are still visible in PDI [2]. In addition, PDI performs equally well in scattering environments where the background light itself is polarized; in this case, proper adjustment of the polarization axes is necessary for feature extraction. Finally, PDI's ability to operate passively, its ease of implementation, and its fast speed render it a practical alternative to conventional imaging.

PDI systems have obvious uses in settings where scattering severely impairs image quality such as in rain, fog, and underwater environments. They can play an important role in automatic target detection and autonomous navigation systems, with possible applications in the military and space exploration. In addition, PDI can be valuable in medical imaging and microscopy where the experimenter can control the polarization of light [3].

1.2 Polarization-Difference Camera

It is the goal of current research to construct a portable polarization-difference camera that can output accurate, high-quality polarization-difference images in real time. While charge-coupled devices (CCD's) are currently the most popular technology for image sensors, we wish to build the camera with CMOS microelectronics that can be fabricated on a single VLSI chip. In addition to its flexibility and cost effectiveness, CMOS technology provides several important advantages over CCD. First, CCD's cannot be easily integrated with CMOS signal processing circuits because of increased complexity and cost. Second, CCD's have limited readout rates inherent in their structure. Finally, CCD's are also easily susceptible to smear and radiation damage [7].

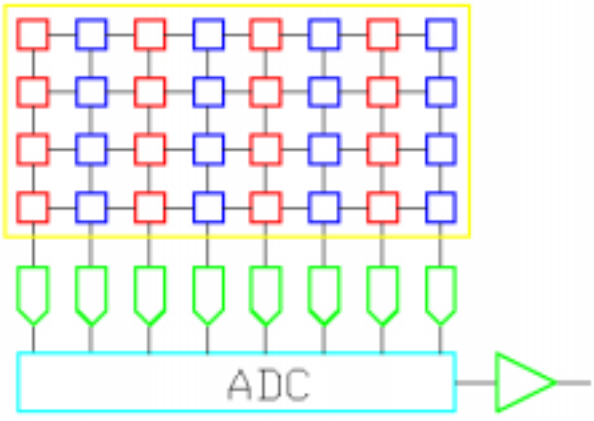

Figure 1.4. Schematic of PDI camera showing pixel array and A-to-D converter (graphic by Gregory Barlow)

The prototype PDI camera will contain a 64×64 pixel array and consist of three main parts: 1) a linear polarization analyzer that will separate incoming light into orthogonal linear components; 2) a CMOS solid-state imager integrating active CMOS pixels with circuitry to process and digitize the signals; and 3) an image display system that will convert the digitized signal output from the CMOS imager to a visible polarization-difference image.

1.2.1. Linear Polarization Analyzer

The PDI camera's precision and high-speed operability are contingent upon the seamless integration of the polarization analyzer with active CMOS microelectronics. The miniaturization and simplification of the system can be accomplished through diffractive optical elements (DOEs), which are passive, compact components that can selectively filter and focus light onto a plane that is only microns away. This paper subsequently describes the analysis and design of DOE lenses that will function as linear polarizers in the PDI camera.

In the circuit schematic shown above, an array of polarization-selective DOEs will be carefully aligned on top of the pixel arrangement. DOEs with a vertical polarization axis will be positioned above the columns of red pixels while DOEs above the blue columns will be oriented in the perpendicular horizontal direction. This allows the DOE matrix to divide incoming light into two distinct components, each predominantly polarized along its overhead DOE's polarization axis, and focus them onto the active pixel sensors below. The size of each DOE will be $18\ \mu m \times 18\ \mu m$ to coordinate with the dimensions of the pixel sensors.

1.2.2. CMOS Solid-State Imager

The first level of the solid-state imager consists of CMOS active pixel image sensors. Active pixel sensors contain one or more active transistors and provide lower noise, improved scalability, and a faster speed readout compared to passive pixels [7]. Their main function is to convert the focused light intensity into electronic signals in current mode. The pixels will then map the electronic signals to on-chip signal processing circuits for addition, subtraction, and scaling of the linearly polarized components. The processed output will pass to an analog-to-digital converter that digitizes the signals for eventual display. Alternatively, the A-to-D converter may be placed immediately after the pixel sensors to digitize the signals before signal-processing circuits perform the necessary calculations.

1.2.3. Image Display System

The image display system will receive the digitized signals and translate the state of polarization into a PDI image. Although gray-scale, monochromatic PDI images such as Figure 1.3(B) can reveal surface features not visible under conventional imaging, they also lose certain details from the polarization-sum image. Ideally, the display system will be able to use colorimetric representations for different polarization states and map the signals into hue, saturation, and intensity. This will effectively combine the information contained in both the polarization-sum and polarization-difference images of a scene.

2. DIFFRACTIVE OPTICAL ELEMENTS

A diffractive optical element (DOE) is a substrate—usually SiO_2 glass—on which complex microstructures have been etched to modulate and transform an incident wave into a predetermined pattern through diffraction. The microstructures' dimensions, typically on the scale of microns, are chosen as a function of wavelength. Examples include Fresnel zone lenses, beam splitters, and polarization analyzers. DOEs have become key components in systems where small dimensions and compactness are necessary and have been used in a growing number of applications including sensor and imaging systems, optical switching, and optical data-storage.

2.1 Diffracting Light

Diffraction is a phenomenon in which wavefronts of propagating waves bend in the presence of obstacles. A DOE controls the diffraction of light by modifying wavefronts through the use of interference and phase control. Always perpendicular to a light wave's direction of propagation, a wavefront is a continuous surface on which the electric and magnetic fields have the same phase and usually the same amplitude. For example, light rays coming from a source at infinity are parallel to each other, and the corresponding wavefront is a flat surface perpendicular to the light rays, also known as a plane wave. When a positive lens focuses a plane wave, it is converted into converging spherical waves centered on the focal point. As an example, an eight-level DOE lens is shown above along with its diffracted light intensity pattern.

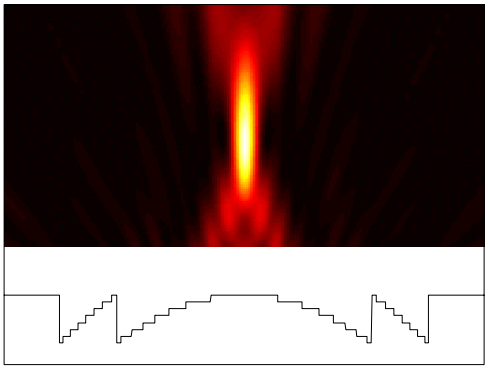

Figure 2.1. A two-zone, 8-level binary optic lens using stepwise approximations to a continuous surface. The lens is illuminated with a TM-polarized plane wave.

2.2 Subwavelength Diffractive Optical Elements

To keep the optical interconnect between the array of DOEs and the array of detectors as compact as possible, the DOEs must be capable of bending light at large angles. This is more easily accomplished through diffraction than refraction, but the DOE's feature sizes must be comparable to the wavelength of the incident wave [8].

DOEs with feature sizes smaller than the wavelength of illumination are called subwavelength diffractive optical elements (SWDOEs). Because of their small feature size, SWDOEs can be designed to perform the same function as multilevel lenses. When an incident light wave approaches the subwavelength grating grooves, diffractive, rather than refractive, optics dominate. The effective index of refraction encountered by the incident wave depends not only on the substrate, but also on the spacing of the grooves and the relative amount of material with respect to air that the wave comes in contact

with. The effective index of refraction seen by the incident wave is therefore a weighted average of the refractive index of the material and that of air. By judiciously selecting the feature sizes and their spacing, one can design a subwavelength lens to implement the same effects of phase control and constructive interference as with a multilevel lens and focus light accordingly, with little loss in performance. An example of a SWDOE is shown in Figure 2.2.

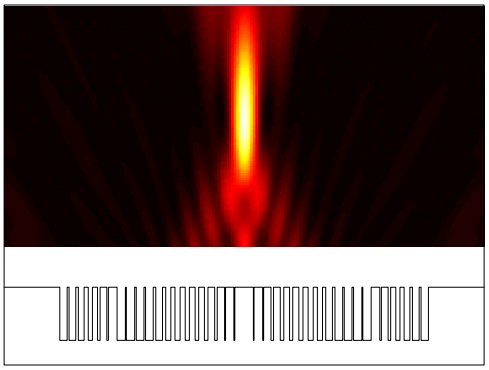

Figure 2.2. Intensity pattern of a binary SWDOE illuminated with a TM polarized plane wave.

In addition to their focusing capabilities, SWDOEs can also function as effective linear polarizers. Their inherently strong polarization-dependence results from the particular direction of the subwavelength gratings, which favors one linear polarization of light over its orthogonal component. The polarization-sensitivity of SWDOEs can be most easily tested by their response to normally-incident transverse magnetic (TM) waves and transverse electric (TE) waves. A wave with TM polarization propagates with the magnetic field perpendicular to the plane of incidence while a TE-polarized wave travels with the electric field perpendicular to the incident plane. As Figure 2.3 shows, the two waves are orthogonally polarized, with the TM wave's electric field perpendicular to the grating grooves and the TE wave's electric field parallel to them. Because of the waves' different polarizations, they encounter different boundary conditions as they approach the SWDOE, resulting in distinct effective indices of refraction [9]. As a result, the phases and efficiencies of the diffracted order can vary greatly. The most important value that quantitatively measures a SWDOE's polarization capability is its intensity ratio, defined as the ratio of the maximum electric field intensity converging on the focal plane for a TM wave versus a TE wave.

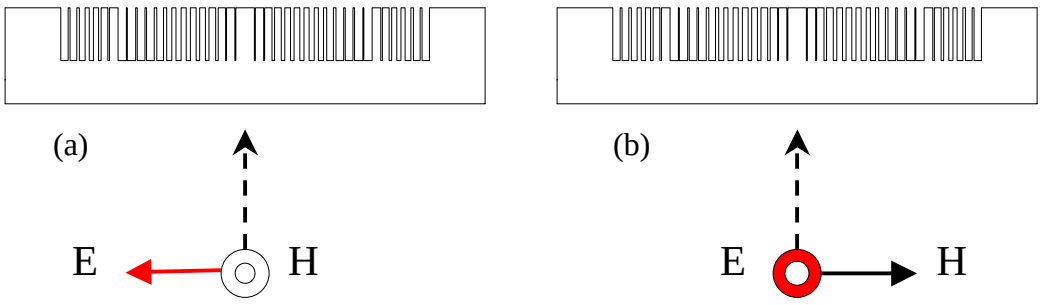

Figure 2.3. The electric field (in red) of (a) the TM-polarized wave is perpendicular to the grooves while (b) the TE wave's electric field is parallel to them.

2.3 Design of Binary Subwavelength Diffractive Lenses

Although some SWDOEs can be designed with analytical techniques, most require the use of an optimization-based synthesis algorithm to determine their optimal profile. Mait,

Prather, and Mirotznik, and Collins have developed procedures to design binary SWDOEs that can emulate the performance of multilevel or continuous-phase DOEs [10].

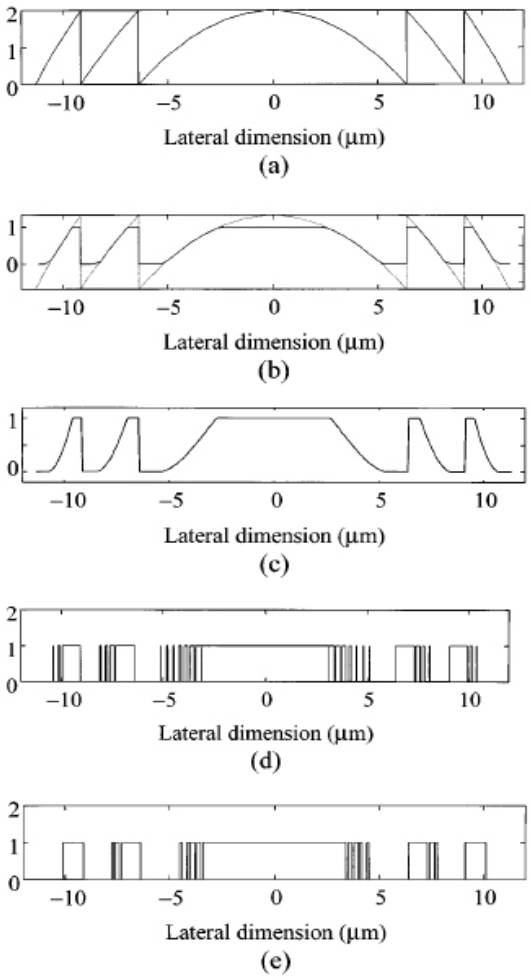

Figure 2.4. (a) Profile of 2π continuous-phase lens. (b) π continuous-phase lens. (c) Index synthesis function used for subwavelength encoding. (d) Binary SWDOE profile. (e) Spatially quantized profile [11].

Prather, Mait, Mirotznik, and Collins also developed the semi-infinite and symmetric boundary element method (SSBEM) as an effective synthesis algorithm. Using this technique to design subwavelength DOEs requires some trial and error, however. The synthesis algorithm is first applied to an initial test

One procedure is based on the com-bination of two approximate theories of dif-fraction - scalar diffraction theory and ef-fective medium theory - and uses the area modulation of subwavelength features [11]. To design a SWDOE that realizes a specific wavefront transformation, the desired super-wavelength function and phase pattern can be mapped onto subwavelength features using the equivalent effective index of re-fraction. Effective medium theory allows one to predict the permittivity of a subwave-length structure, and consequently its rela-tive effective index of refraction $n(x)$. Scalar diffraction theory, on the other hand, determines the phase transformation of a wave field $\theta(x)$ given a relative index of refraction. Together, the two theories will allow one to predict the phase transforma-tion $\theta(x)$ given a particular profile $f(x)$ and, through manipulation of formulas, vice versa. Subwavelength encoding of a con-tinuous function is performed using a process called pulse-width modulation [11]. This process relates area to phase, and the desired change in phase $\theta(x)$ determines the minimum feature size that is necessary to generate the phase accurately. However, if the required feature size is smaller than what current technology can fabricate, the DOE profile must be spatially quantized, which leads to a small decrease in diffraction efficiency (Figure 2.4).

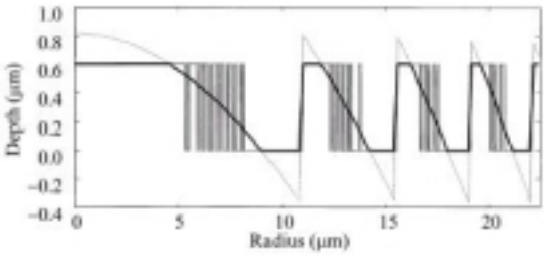

Figure 2.5. Mapping of continuous-phase profile into binary subwavelength features [8].

profile to model its forward wave propagation on a focal plane. Evaluation of its performance will allow the optimization routine to determine necessary changes to the profile. The synthesis algorithm is then applied again to the new profile to model its wave propagation, and the process is repeated until the performance of the DOE is acceptable [10]. To generate the final optimized profile, many iterations of simulated annealing and quenching must be performed computationally and may require significant amounts of memory and time. Figures 2.4 and 2.5 show the encoding process from a continuous phase function to subwavelength features. For more information on binary SWDOE design, see [10] and [11].

2.4 Finite-Difference Time-Domain Method

As the feature sizes of diffractive optical elements become comparable to optical wavelengths, conventional methods of analysis no longer apply due to the increasing effects of electromagnetic coupling along the surface boundaries. As a result, the rigorous solution of Maxwell's equations must be obtained from numerical techniques. Several rigorous methods have been developed, but each has its limitations. For example, rigorous coupled-wave analysis can be applied only to periodic gratings while the finite-element, boundary-element, and finite-difference methods are restricted to the analysis of one-dimensional structures because of their computational demand. Analyzing two-dimensional structures requires a practical three-dimensional solution of Maxwell's equations [4].

K. S. Yee first proposed the finite-difference time-domain (FDTD) method in his 1966 paper [5], but it was largely overlooked because the inadequate computing power of the time precluded its practical implementation. However, in the past decade, FDTD has been resurrected as one of the most widely used numerical techniques for solving electromagnetic problems.

The FDTD method, as its name suggests, finds a direct finite-difference approximation to Maxwell's time-dependent curl equations. By expanding these equations in a 3D rectangular coordinate system, one can transform them into an equivalent system of six coupled scalar equations for all electric and magnetic field components. These 3D equations are used to construct a sampled grid of cells called Yee cells, which in turn allow the modeling of complex geometries composed of different materials. The unknown field distribution over a finite space is then calculated using a time-marching algorithm that propagates the electric and magnetic fields at successive time steps [4].

The FDTD method offers three main advantages over other numerical methods: 1) it is a complete and direct solution of Maxwell's time-domain equations, avoiding superfluous approximations; 2) it can be applied to a wide variety of materials and geometries; and 3) it demands less memory and computational resources. Its main disadvantage usually lies in its requirement that all structures fit a Cartesian grid; therefore, all curved surfaces must be approximated by stepwise functions, which inevitably introduce some inaccuracy. Nevertheless, it should be noted that significant research is underway to

overcome this shortfall. For the complete mathematical derivation of the FDTD method, see [4] and [5].

All DOE design and analyses described in this paper were performed using the FDTD method with Matlab software developed by Dr. Shouyuan Shi and Dr. Dennis Prather of the University of Delaware.

3. PROBLEM STATEMENT AND DESIGN CONSIDERATIONS

The research effort described in this paper is aimed towards designing an optimal substrate profile for a 2D binary subwavelength diffractive lens that will function as a linear polarizer for incident waves in the visible spectrum. A number of physical constraints and performance criteria must be satisfied in the final design.

First, the dimensions of the DOE must match that of the CMOS active pixel sensors and the area of the detector, allowing the proper integration of the components. The lens must be accurately designed for a specific focal length that is equivalent to its distance from the array of pixel sensors, its focal plane. The profile of the lens must also conform to fabrication constraints; i. e., the minimum feature size and maximum etch depth must be computationally and physically realizable.

A number of variables can be used to measure the performance of a SWDOE, the most important of which is the intensity ratio for the purposes of this project. A higher intensity ratio of TM vs. TE waves indicates superior polarization filtering capability (Figure 3.1). To ensure consistency in the camera's performance, it is also preferable that the intensity ratio remains relatively constant across the wavelengths of the visible spectrum, namely, from 300 nm to 700 nm. As Figure 3.1 shows, plots of the electric

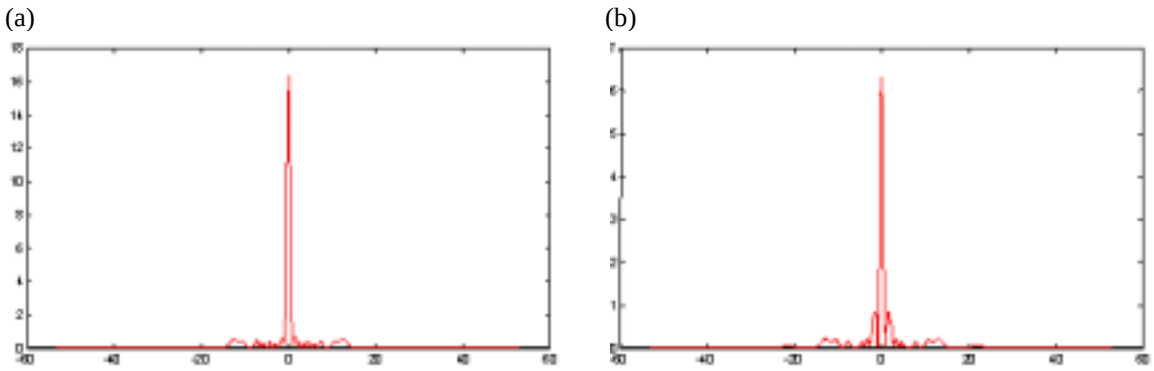

Figure 3.1. (a) TM- and (b)TE-wave electric field intensity plots on the focal plane produced by an SWDOE designed for 500 nm waves. The x-axis is normalized with respect to the DOE's operating wavelength; i. e., 60 units equals 30μm. The intensity axis is normalized with respect to the intensity of the illuminating wave. This particular example indicates an intensity ratio of approximately 16:6.

field intensity on the focal plane should also resemble a delta function as closely possible; that is, ideally, the intensity should be at a maximum on the focal axis and approach zero elsewhere. The minimization of side lobes reflects a strong focusing capability and

prevents one DOE's transmitted light pattern from bleeding over onto adjacent pixels. The design of the lens must also account for aberrations in the incoming light's angle of incidence. While the light rays are assumed to approach the DOE at an angle perpendicular to the length of the substrate, the performance of the DOE should be tolerant to small deviations of no more than 10°. Lastly, diffraction efficiency, defined as the ratio of energy within a specific interval on the focal plane to the total energy that is incident upon the SWDOE, should be maximized for TM versus TE waves.

4. EXPERIMENTAL RESULTS

4.1 Initial Analysis

We began the analysis of SWDOEs by examining the effects of changing single variables, specifically the number of zones, the index of refraction, and wavelength of illumination. An initial lens was designed for the 500 nm wavelength, and its number of zones was changed from one to six while keeping the focal length at 5 μm. To examine these effects on polarization sensitivity, we separately illuminated each lens by a TM wave and a TE wave with varying wavelengths in the visible spectrum. Figure 4.1 shows the results.

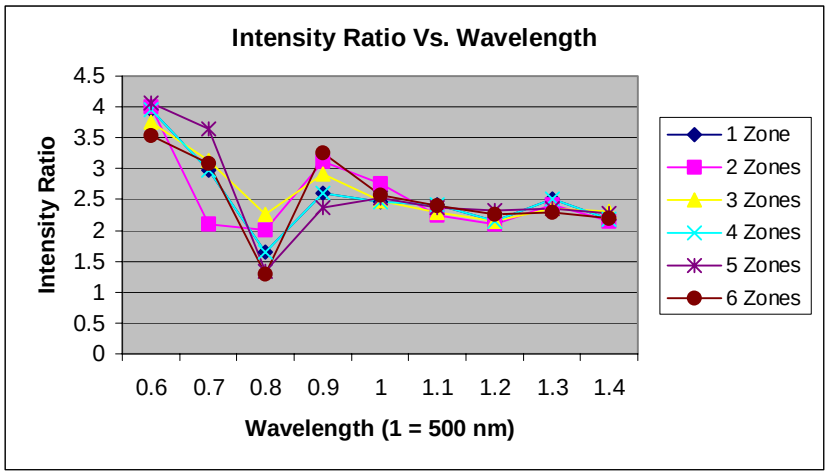

Figure 4.1. Intensity ratio vs. wavelength plot for 500 nm SWDOEs with varying numbers of zones. See Appendix A for table of values.

The graph indicates that the number of zones in a DOE does not have a significant impact on the intensity ratio since the lens tested above all exhibit approximately the same pattern for the various wavelengths. One characteristic of the plot worth noting is the common peak when the lenses were illuminated with a 300 nm wave and the common minimum for a 400 nm wave. This results from resonance effects that occur when the illuminating wavelength is a specific multiple of the DOE's minimum feature size.

Although the number of zones does not significantly affect the intensity ratio, Figure 4.2 shows that the diffraction efficiency generally decreases as the number of zones increases. This could be a result of the fact that zones in subwavelength lenses are only

approximations to continuous phase functions; an increase in the number of zones therefore introduces more approximation in the focusing ability of the lens.

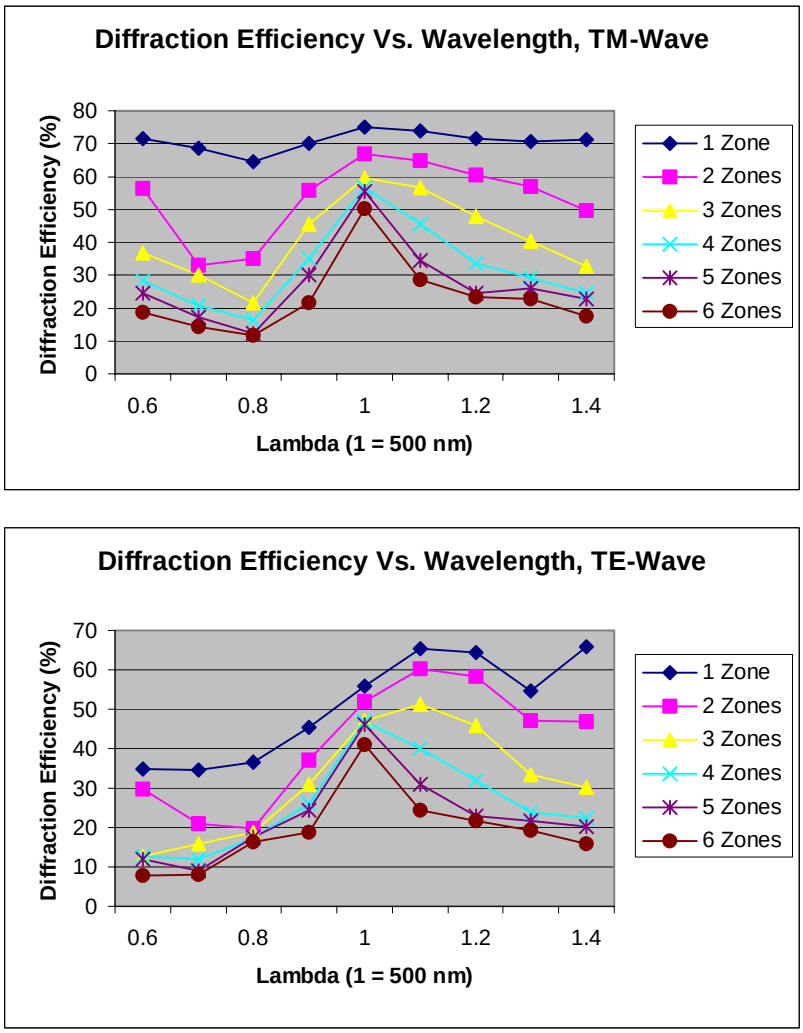

Figure 4.2. Diffraction Efficiency versus wavelength for a 500 nm SWDOE. The top and bottom graphs show the response to TM- and TE-wave illumination, respectively.

As the above graphs show, the diffraction efficiency typically reaches a maximum when the lenses are illuminated with 500 nm waves. This is not surprising since the DOEs were designed for that wavelength. Unfortunately, the diffraction efficiency and absolute intensity drop sharply as the illuminating wavelength strays from 500 nm, primarily because the focal length effectively changes when a lens is not hit with the wavelength it was designed for. As Figure 4.3 shows, a 400 nm light wave overshoots its intended focal plane, while the 700 nm wave converges a few microns short of the focal plane. In addition, large differences between the illuminating light's wavelength and the DOE's operating wavelength can dramatically increase the size of the side lobes in the focal

plane intensity plot (Figure 4.4). These inherent limitations also exist in all subsequent DOE designs.

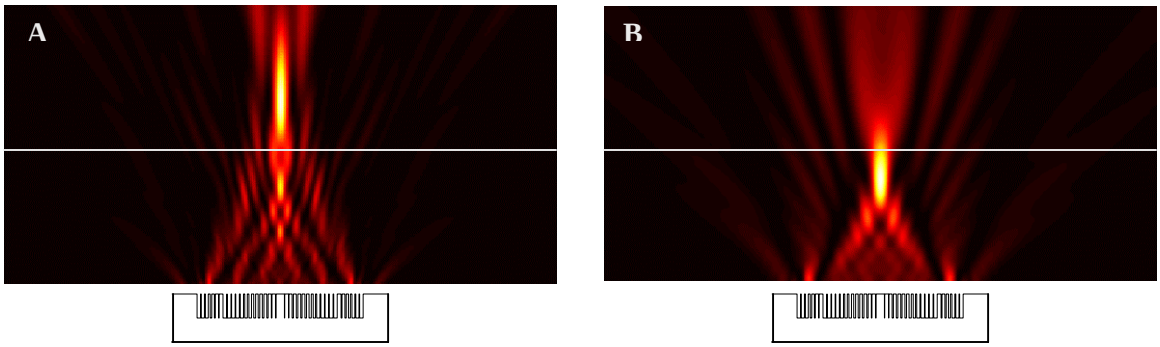

Figure 4.3. A DOE designed for 500 nm waves is illuminated with a A) 400 nm wave and B) 700 nm wave. The region with the highest intensity does not fall on the focal plane.

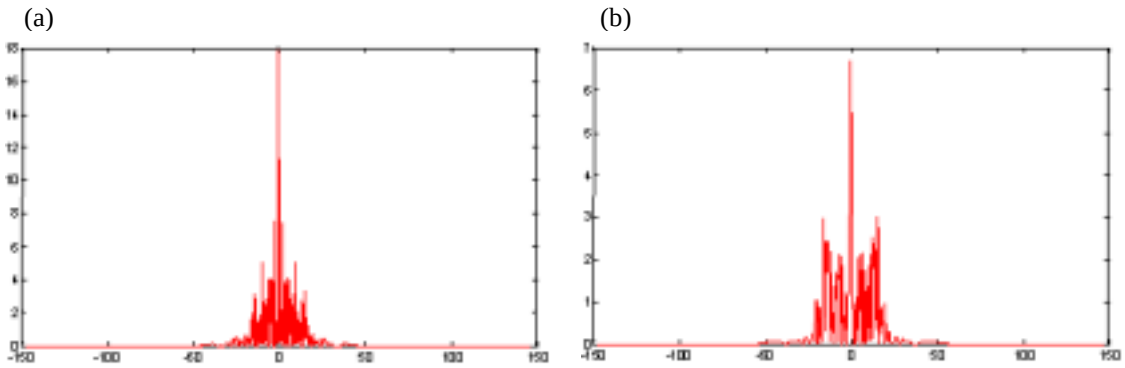

Figure 4.4. Focal plane electric field intensity plots for a 500 nm SWDOE when it is illuminated by a (a) 300 nm TM-wave and (b) 700 nm TM-wave. Compare with Figure 3.1, where the side lobes are virtually nonexistent.

We also tested 500 nm binary SWDOEs etched in substrates with different indices of refraction, from $n = 1.5$ to $n = 4$. Figure 4.5 reveals that while substrates with higher indices of refraction are capable of producing much higher intensity ratios, the ratios fluctuate wildly across the visible spectrum. Furthermore, substrates with high indices of refraction are not readily available; the most common is SiO_2 glass, which has a refractive index of 1.5.

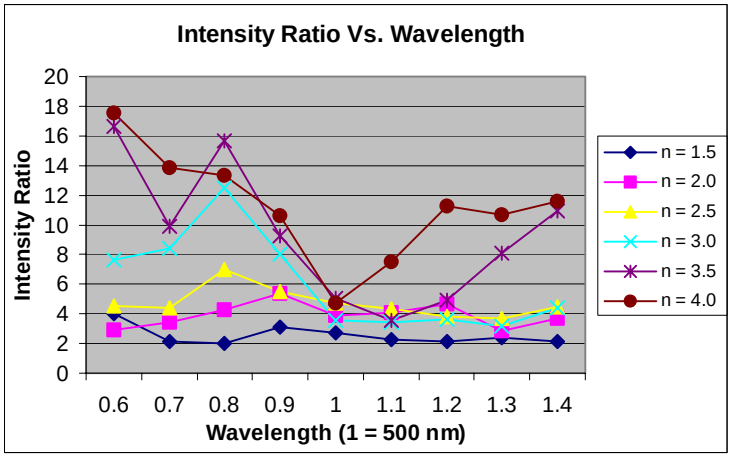

Figure 4.5. Intensity ratio vs. wavelength plot for 500 nm SWDOEs with varying indices of refraction. See Appendix B for table of values.

4.2 Design of Subwavelength Diffractive Lenses With Final Dimensions

While the initial analysis involved only lenses designed for the 500 nm wavelength, subsequent analyses tested the performance of lenses designed for other wavelengths of the visible spectrum. In addition, after the size of the active pixel sensors was finalized to be 18μm × 18μm, these dimensions were applied as constraints to the DOE design. For each lens designed for a particular wavelength, the number of zones was chosen so that the overall length of the profile would not exceed 18 μm. (See Appendix C for complete specifications of these lenses.)

Figure 4.6 shows the intensity ratio vs. wavelength plots of lenses designed for the 300 nm, 400nm, 500 nm, 600 nm, and 700 nm wavelengths along with their absolute intensity plots. The profile of each DOE measured approximately 18 μm across, and focal length was chosen arbitrarily to be 6 μm.

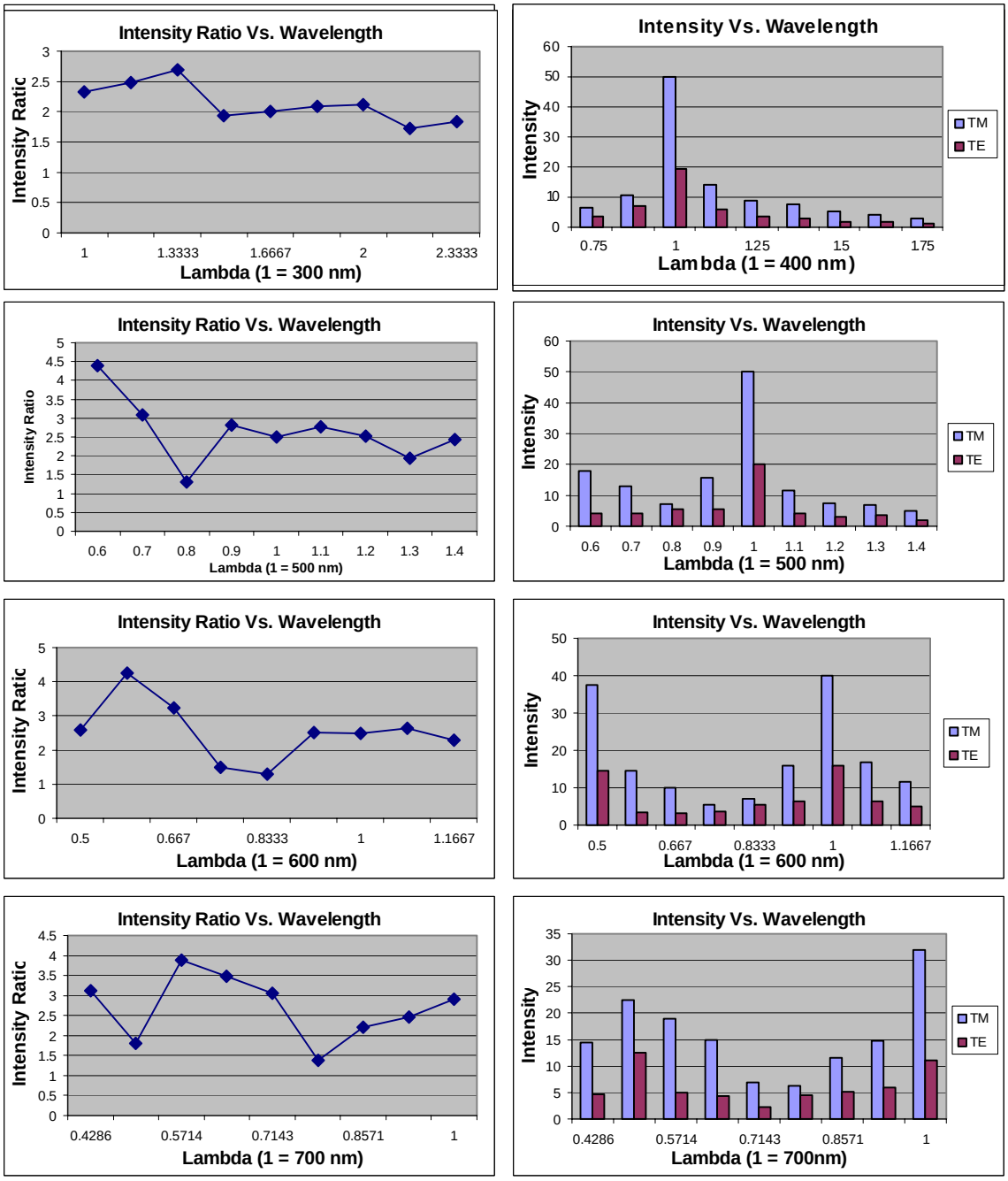

Figure 4.6. Intensity ratio vs. wavelength and intensity vs. wavelength plots for SWDOEs designed for 300 – 700 nm waves.

Ideally, the lens should be fabricated for 600 nm incident waves because the active pixel sensors achieve the highest quantum efficiency at that wavelength. Therefore, the DOE operating at 300 nm would not function well since the detector will not be likely to collect its full, transmitted intensity. Evaluation of the focal plane intensity plots for the

five lenses above revealed that the 400 nm and 500 nm lenses appeared to produce the smallest side lobes and are therefore the most desirable.

To determine whether the 400 nm and 500 nm lenses could be further refined, we designed a DOE to operate at the 450 nm wavelength. Its intensity ratio vs. wavelength and absolute intensity vs. wavelength plots are shown in Figure 4.7. The 450 nm lens exhibits properties very similar to those of the 400 nm and 500 nm lenses, but it seems to produce slightly lower side lobes for the visible wavelengths. The 450 nm lens was subsequently tested for its tolerance to deviations in the incident wave's angle of incidence. Figure 4.8 shows that for waves incident at 80°, the lens still performs effectively with a very slight shift from the focal axis given a focal length of 6 μm. However, as the focal length increases, small changes in a wave's angle of incidence can cause exaggerated shifting of the focused intensity away from the axis.

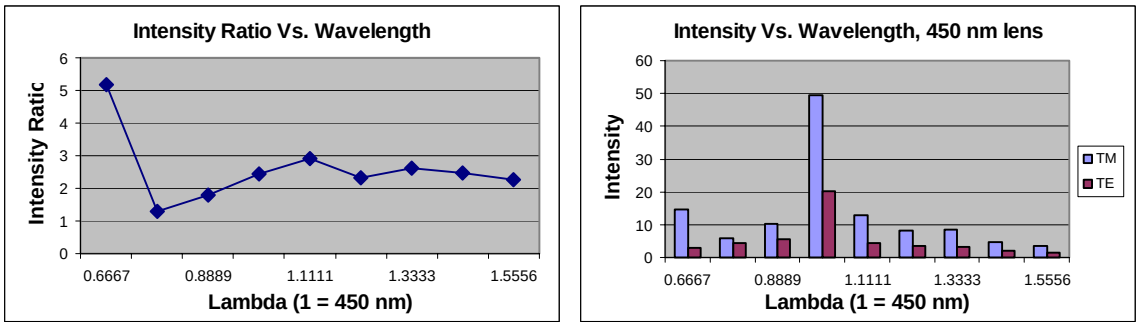

Figure 4.7. Intensity ratio vs. wavelength and absolute intensity vs. wavelength plots for a 450 nm SWDOE. See Appendix C for complete table of values.

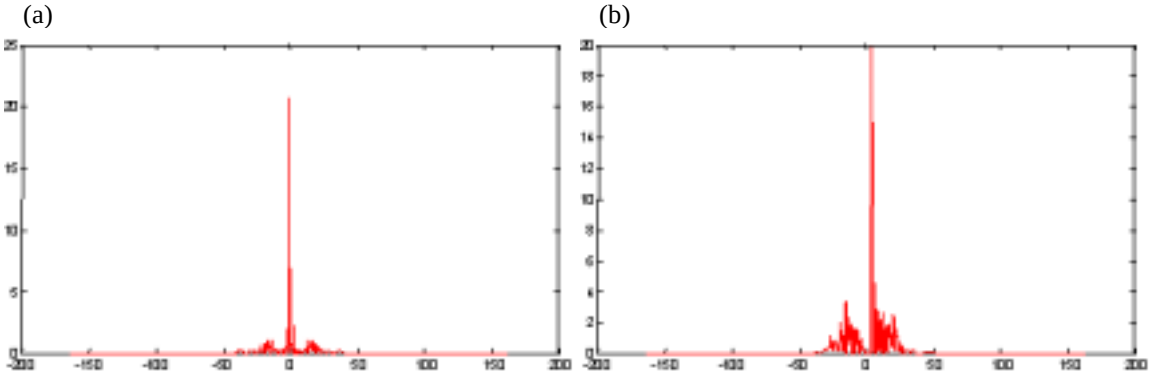

Figure 4.8. The 450 nm lens is illuminated with a 450 nm TM-wave at (a) 90° angle of incidence and (b) 80° angle of incidence. In plot (b), the peak intensity is shifted slightly to the right of the focal axis.

5. DISCUSSION AND CONCLUSIONS

The above analyses show that no single SWDOE exhibits superior performance in all design criteria; instead, there are many tradeoffs among the various factors which the

designer needs to carefully weigh. For example, lenses with high indices of refraction can achieve intensity ratios of up to 17:1, but their performance is volatile and unpredictable. On the other hand, while the 300 nm lens displays a very consistent intensity ratio across the visible wavelengths of light, it is not a suitable choice given the quantum efficiency distribution of the active pixel sensors. The most effective and consistent lenses appear to be the 400, 450, and 500 nm DOEs since they exhibit relatively low side lobes when operating outside of their designated wavelength and also provide a fairly constant intensity ratio of approximately 2.5:1. However, all the lenses tested show a steep drop in absolute intensity when not illuminated with their intended wavelength.

6. RECOMMENDATIONS

The DOE designs and analyses discussed in this paper still await rounds of fabrication and experimental verification before a final profile can be implemented. This paper is primarily concerned with the design of a simple polarization analyzer for use in a prototype PDI camera, and therefore only investigated isotropic substrates containing binary subwavelength profiles. However, it would be beneficial in the future to research multilayer, anisotropic polarizers, which are structures of much higher complexity but also of correspondingly greater performance.

In addition, while the subwavelength structures described here are two-dimensional structures that focus light along a center line parallel to its grooves, one can employ more sophisticated design methods to allow focusing onto a point. It would also be preferable in the future to fabricate a polarizing beam splitter that can automatically separate incoming light into orthogonal components and focus them at two distinct points.

7. ACKNOWLEDGEMENTS

I would like to thank Dr. Nader Engheta for introducing me to the field of electromagnetism and optics and giving me the opportunity to conduct research on polarization-difference imaging. His enduring enthusiasm, patience, and guidance have been a great inspiration. I would like to thank Dr. Dennis Prather of the University of Delaware for providing me with in-depth knowledge on diffractive optical elements along with the software tools needed for their design and analysis. I would also like to thank Dr. Jan Van der Spiegel and the National Science Foundation for organizing and funding this undergraduate research program. Also, many thanks to Gregory Barlow, my summer roommate and research partner who helped me with various aspects of my project. Finally, thanks to the entire SUNFEST gang for making this summer as enjoyable as it was instructive.

8. REFERENCES

1. M. P. Rowe, N. Engheta, S. S. Easter, Jr., E. N. Pugh, Jr., "Graded-index model of a fish double cone exhibits differential polarization sensitivity," J. Opt. Soc. Am. A **11**, 55-69 (1994).
2. M. P. Rowe, E. N. Pugh, Jr., J. S. Tyo, N. Engheta, "Polarization-difference imaging: a biologically inspired technique for observation through scattering media," Opt. Lett. **20**, 608-610 (1995).
3. J. S. Tyo, M. P. Rowe, E. N. Pugh, Jr., N. Engheta, "Target detection in optically scattering media by polarization-difference imaging," Appl. Opt. **35**, 1855-1870 (1996).
4. M. S. Mirotznik, D. W. Prather, J. N. Mait, et al, "Three-dimensional analysis of subwavelength diffractive optical elements with the finite-difference time-domain method," Appl. Opt. **39**, 2871-2880 (2000).
5. K. S. Yee, "Numerical solution of initial boundary value problems involving Maxwell's equations in isotropic media," IEEE Trans. Ant. Prop., AP **14**, 302-307 (1966).
6. U. S. Inan, Aziz S. Inan, *Electromagnetic Waves*, Prentice Hall, Upper Saddle River, New Jersey, 2000.
7. S. K. Mendis, S. E. Kemeny, R. C. Gee et al, "CMOS active pixel image sensors for highly integrated imaging systems," IEEE Journal of Solid-State Circuits **32**, 187-188 (1997).
8. J. N. Mait, A. Scherer, O. Dial, et al, "Diffractive lens fabricated with binary features less than 60 nm," Opt. Lett. **25**, 381-383 (2000).
9. R. C. Tyan, A. A. Salvekar, H. P.Chou, et al, "Design, fabrication, and characterization of form-birefringent multiplayer polarizing beam splitter," J. Opt. Soc. Am. A **14**, 1627-1635 (1997).
10. D. W. Prather and J. N. Mait, M. S. Mirotznik, and J. P. Collins, "Vector-based synthesis of finite aperiodic subwavelength diffractive optical elements," J. Opt. Soc. Am. A **15**, 1599-1606 (1998).
11. J. N. Mait, D. W. Prather, M. S. Mirotznik, "Binary subwavelength diffractive-lens design," Opt. Lett. **23**, 1343-1345 (1998).

APPENDIX A

Focus	10		10		10		10		10		10		10		10		10	
lambda (lens)	1		1		1		1		1		1		1		1		1	
zones	1		1		1		1		1		1		1		1		1	
index	1.5		1.5		1.5		1.5		1.5		1.5		1.5		1.5		1.5	
lambda	0.6		0.7		0.8		0.9		1		1.1		1.2		1.3		1.4	
angle	90		90		90		90		90		90		90		90		90	
samp rate	20		20		20		20		20		20		20		20		20	
mode	TM	TE	TM	TE	TM	TE	TM	TE	TM	TE	TM	TE	TM	TE	TM	TE	TM	TE
efficiency	71.52	34.8	68.5	34.65	64.65	36.47	70.08	45.36	75.18	55.87	73.94	65.32	71.52	64.47	70.53	54.58	71.17	65.76
intensity	17.5	3.6	14	3	10	2.5	10.5	3	9.8	3.25	7.5	3	6.25	2.7	5.8	2.2	6.25	2.8
intensity ratio	4.861111111		4.666666667		4		3.5		3.015384615		2.5		2.314814815		2.636363636		2.232142857	

Focus	10		10		10		10		10		10		10		10		10	
lambda (lens)	1		1		1		1		1		1		1		1		1	
zones	2		2		2		2		2		2		2		2		2	
index	1.5		1.5		1.5		1.5		1.5		1.5		1.5		1.5		1.5	
lambda	0.6		0.7		0.8		0.9		1		1.1		1.2		1.3		1.4	
angle	90		90		90		90		90		90		90		90		90	
samp rate	20		20		20		20		20		20		20		20		20	
mode	TM	TE	TM	TE	TM	TE	TM	TE	TM	TE	TM	TE	TM	TE	TM	TE	TM	TE
efficiency	56.44	29.66	33.1	21.07	34.95	19.78	55.74	36.98	66.98	51.96	64.76	60.13	60.53	58.36	56.94	47.05	49.53	46.87
intensity	24	6	8	3.8	6.25	3.1	14	4.5	16.5	6	13	5.8	10	4.75	8.7	3.6	7	3.25
intensity ratio	4		2.105263158		2.016129032		3.111111111		2.75		2.24137931		2.105263158		2.416666667		2.153846154	

Focus	10		10		10		10		10		10		10		10		10	
lambda (lens)	1		1		1		1		1		1		1		1		1	
zones	3		3		3		3		3		3		3		3		3	
index	1.5		1.5		1.5		1.5		1.5		1.5		1.5		1.5		1.5	
lambda	0.6		0.7		0.8		0.9		1		1.1		1.2		1.3		1.4	
angle	90		90		90		90		90		90		90		90		90	
samp rate	20		20		20		20		20		20		20		20		20	
mode	TM	TE	TM	TE	TM	TE	TM	TE	TM	TE	TM	TE	TM	TE	TM	TE	TM	TE
efficiency	36.69	12.77	29.95	15.91	21.58	18.78	45.48	31.09	59.44	47.01	56.62	51.12	47.93	45.94	40.17	33.32	32.79	30.19
intensity	15	4	12.5	4	7.9	3.5	14	4.8	21	8.5	16	7	10.5	4.9	6.8	2.9	4.6	2
intensity ratio	3.75		3.125		2.257142857		2.916666667		2.470588235		2.285714286		2.142857143		2.344827586		2.3	

Focus	10		10		10		10		10		10		10		10		10	
lambda (lens)	1		1		1		1		1		1		1		1		1	
zones	4		4		4		4		4		4		4		4		4	
index	1.5		1.5		1.5		1.5		1.5		1.5		1.5		1.5		1.5	
lambda	0.6		0.7		0.8		0.9		1		1.1		1.2		1.3		1.4	
angle	90		90		90		90		90		90		90		90		90	
samp rate	20		20		20		20		20		20		20		20		20	
mode	TM	TE	TM	TE	TM	TE	TM	TE	TM	TE	TM	TE	TM	TE	TM	TE	TM	TE
efficiency	28.3	12.66	20.6	11.95	16.48	17.22	34.99	26.19	56.62	46.95	45.62	39.92	33.58	31.98	29.21	23.93	24.67	22.33
intensity	17	4.3	9.8	3.3	6.9	4.2	13.5	5.2	27	11	15	6.2	7.5	3.5	6	2.4	5.9	2.7
intensity ratio	3.953488372		2.96969697		1.642857143		2.596153846		2.454545455		2.419354839		2.142857143		2.5		2.185185185	

APPENDIX A

Focus	10		10		10		10		10		10		10		10		10	
lambda (lens)	1		1		1		1		1		1		1		1		1	
zones	5		5		5		5		5		5		5		5		5	
index	1.5		1.5		1.5		1.5		1.5		1.5		1.5		1.5		1.5	
lambda	0.6		0.7		0.8		0.9		1		1.1		1.2		1.3		1.4	
angle	90		90		90		90		90		90		90		90		90	
samp rate	20		20		20		20		20		20		20		20		20	
mode	TM	TE	TM	TE	TM	TE	TM	TE	TM	TE	TM	TE	TM	TE	TM	TE	TM	TE
efficiency	24.43	11.93	17.19	9.12	12.4	17.55	30.11	24.39	55.61	45.98	34.55	30.95	24.4	23.04	26.03	21.81	22.68	20.28
intensity	17.5	4.3	10	2.75	7	5.25	13	5.5	34	13.5	11.8	5	6.5	2.8	7.5	3.2	7.5	3.3
intensity ratio	4.069767442		3.636363636		1.333333333		2.363636364		2.518518519		2.36		2.321428571		2.34375		2.272727273	

Focus	10		10		10		10		10		10		10		10		10	
lambda (lens)	1		1		1		1		1		1		1		1		1	
zones	6		6		6		6		6		6		6		6		6	
index	1.5		1.5		1.5		1.5		1.5		1.5		1.5		1.5		1.5	
lambda	0.6		0.7		0.8		0.9		1		1.1		1.2		1.3		1.4	
angle	90		90		90		90		90		90		90		90		90	
samp rate	20		20		20		20		20		20		20		20		20	
mode	TM	TE	TM	TE	TM	TE	TM	TE	TM	TE	TM	TE	TM	TE	TM	TE	TM	TE
efficiency	18.58	7.88	14.19	8.12	11.59	16.43	21.68	18.7	50.22	40.92	28.71	24.37	23.31	21.66	22.74	19.26	17.49	15.91
intensity	15	4.25	10	3.25	7.1	5.5	13.8	4.25	36	14	10.2	4.25	7.9	3.5	7.8	3.4	5.5	2.5
intensity ratio	3.529411765		3.076923077		1.290909091		3.247058824		2.571428571		2.4		2.257142857		2.294117647		2.2	

APPENDIX B

Focus	10		10		10		10		10		10		10		10		10	
lambda (lens)	1		1		1		1		1		1		1		1		1	
zones	2		2		2		2		2		2		2		2		2	
index	1.5		1.5		1.5		1.5		1.5		1.5		1.5		1.5		1.5	
lambda	0.6		0.7		0.8		0.9		1		1.1		1.2		1.3		1.4	
angle	90		90		90		90		90		90		90		90		90	
samp rate	20		20		20		20		20		20		20		20		20	
mode	TM	TE	TM	TE	TM	TE	TM	TE	TM	TE	TM	TE	TM	TE	TM	TE	TM	TE
efficiency	56.44	29.66	33.1	21.07	34.95	19.78	55.74	36.98	66.98	51.96	64.76	60.13	60.53	58.36	56.94	47.05	49.53	46.87
intensity	24	6	8	3.8	6.25	3.1	14	4.5	16.5	6	13	5.8	10	4.75	8.7	3.6	7	3.25
intensity ratio	4		2.105263158		2.016129032		3.111111111		2.75		2.24137931		2.105263158		2.416666667		2.153846154	

Focus	10		10		10		10		10		10		10		10		10	
lambda (lens)	1		1		1		1		1		1		1		1		1	
zones	2		2		2		2		2		2		2		2		2	
index	2		2		2		2		2		2		2		2		2	
lambda	0.6		0.7		0.8		0.9		1		1.1		1.2		1.3		1.4	
angle	90		90		90		90		90		90		90		90		90	
samp rate	20		20		20		20		20		20		20		20		20	
mode	TM	TE	TM	TE	TM	TE	TM	TE	TM	TE	TM	TE	TM	TE	TM	TE	TM	TE
efficiency	27.65	27.1	32.45	21.26	29.69	21.17	53.9	31.06	51.5	38.9	58.96	47.83	53.92	41	49.66	56.69	43.85	41.12
intensity	9.6	3.3	7.5	2.2	9	2.1	14	2.6	12	3.1	12.25	3	14	3	9.5	3.3	7.8	2.1
intensity ratio	2.909090909		3.409090909		4.285714286		5.384615385		3.870967742		4.083333333		4.666666667		2.878787879		3.714285714	

Focus	10		10		10		10		10		10		10		10		10	
lambda (lens)	1		1		1		1		1		1		1		1		1	
zones	2		2		2		2		2		2		2		2		2	
index	2.5		2.5		2.5		2.5		2.5		2.5		2.5		2.5		2.5	
lambda	0.6		0.7		0.8		0.9		1		1.1		1.2		1.3		1.4	
angle	90		90		90		90		90		90		90		90		90	
samp rate	20		20		20		20		20		20		20		20		20	
mode	TM	TE	TM	TE	TM	TE	TM	TE	TM	TE	TM	TE	TM	TE	TM	TE	TM	TE
efficiency	25.78	22.37	25.24	16.64	29.78	18.24	43.08	21.09	43.02	36.11	45.15	48.94	42.89	54.93	39.81	49.03	37.79	36.37
intensity	12.25	2.7	7	1.6	10.5	1.5	8	1.45	8	1.7	13	3	8.8	2.3	7.8	2.1	6.7	1.5
intensity ratio	4.537037037		4.375		7		5.517241379		4.705882353		4.333333333		3.826086957		3.714285714		4.466666667	

Focus	10		10		10		10		10		10		10		10		10	
lambda (lens)	1		1		1		1		1		1		1		1		1	
zones	2		2		2		2		2		2		2		2		2	
index	3		3		3		3		3		3		3		3		3	
lambda	0.6		0.7		0.8		0.9		1		1.1		1.2		1.3		1.4	
angle	90		90		90		90		90		90		90		90		90	
samp rate	20		20		20		20		20		20		20		20		20	
mode	TM	TE	TM	TE	TM	TE	TM	TE	TM	TE	TM	TE	TM	TE	TM	TE	TM	TE
efficiency	27.71	15.13	21.86	18.1	27.92	14.2	27.65	24.63	33.16	42.34	28.37	45.39	31.16	52.74	30.12	49.65	26.61	41.85
intensity	11.5	1.5	6.5	0.77	7.5	0.6	6	0.75	6	1.7	6.5	1.9	4.75	1.3	4.25	1.35	4.4	1
intensity ratio	7.666666667		8.441558442		12.5		8		3.529411765		3.421052632		3.653846154		3.148148148		4.4	

APPENDIX B

Focus	10		10		10		10		10		10		10		10		10	
lambda (lens)	1		1		1		1		1		1		1		1		1	
zones	2		2		2		2		2		2		2		2		2	
index	3.5		3.5		3.5		3.5		3.5		3.5		3.5		3.5		3.5	
lambda	0.6		0.7		0.8		0.9		1		1.1		1.2		1.3		1.4	
angle	90		90		90		90		90		90		90		90		90	
samp rate	20		20		20		20		20		20		20		20		20	
mode	TM	TE	TM	TE	TM	TE	TM	TE	TM	TE	TM	TE	TM	TE	TM	TE	TM	TE
efficiency	20.28	12.77	17.97	12.85	23.61	18.32	21.65	21.27	22.34	36.61	24.9	46.3	22.58	35.56	20.36	28.4	21.88	20.5
intensity	5	0.3	4.25	0.43	5.8	0.37	5.2	0.56	3.4	0.67	4.1	1.15	3.2	0.65	2.1	0.26	2.4	0.22
intensity ratio	16.66666667		9.88372093		15.67567568		9.285714286		5.074626866		3.565217391		4.923076923		8.076923077		10.90909091	

Focus	10		10		10		10		10		10		10		10		10	
lambda (lens)	1		1		1		1		1		1		1		1		1	
zones	2		2		2		2		2		2		2		2		2	
index	4		4		4		4		4		4		4		4		4	
lambda	0.6		0.7		0.8		0.9		1		1.1		1.2		1.3		1.4	
angle	90		90		90		90		90		90		90		90		90	
samp rate	20		20		20		20		20		20		20		20		20	
mode	TM	TE	TM	TE	TM	TE	TM	TE	TM	TE	TM	TE	TM	TE	TM	TE	TM	TE
efficiency	18.78	8.33	21.24	15.23	18.84	11.59	19.84	35.91	17.51	36.53	19.01	27.74	17.75	20.56	20.33	20.94	22.52	22.62
intensity	5.7	0.325	6.5	0.47	4	0.3	5.3	0.5	3.75	0.79	2.25	0.3	2.25	0.2	2.56	0.24	2.6	0.225
intensity ratio	17.53846154		13.82978723		13.33333333		10.6		4.746835443		7.5		11.25		10.66666667		11.55555556	

APPENDIX C

Focus	20		20		20		20		20		20		20		20		20	
lambda (lens)	1		1		1		1		1		1		1		1		1	
zones	16		16		16		16		16		16		16		16		16	
index	1.5		1.5		1.5		1.5		1.5		1.5		1.5		1.5		1.5	
lambda (1 = 300 nm)	1		1.1667		1.3333		1.5		1.6667		1.8333		2		2.1667		2.3333	
angle	90		90		90		90		90		90		90		90		90	
samp rate	20		20		20		20		20		20		20		20		20	
mode	TM	TE	TM	TE	TM	TE	TM	TE	TM	TE	TM	TE	TM	TE	TM	TE	TM	TE
efficiency	38.3344	34.68	11.952	9.466	7.781	5.9024	6.8021	6.7882	5.3469	4.4491	5.4675	4.5275	4.7919	4.9011	4.692	5.5742	4.5276	5.1972
intensity	70	30	14.6	5.9	7.4	2.75	6	3.1	3.6	1.8	3.75	1.8	2.75	1.3	2.25	1.3	2.65	1.44
intensity ratio	2.333333333		2.474576271		2.690909091		1.935483871		2		2.083333333		2.115384615		1.730769231		1.840277778	

Focus	15		15		15		15		15		15		15		15		15	
lambda (lens)	1		1		1		1		1		1		1		1		1	
zones	12		12		12		12		12		12		12		12		12	
index	1.5		1.5		1.5		1.5		1.5		1.5		1.5		1.5		1.5	
lambda (1 = 400 nm)	0.75		0.875		1		1.125		1.25		1.375		1.5		1.625		1.75	
angle	90		90		90		90		90		90		90		90		90	
samp rate	20		20		20		20		20		20		20		20		20	
mode	TM	TE	TM	TE	TM	TE	TM	TE	TM	TE	TM	TE	TM	TE	TM	TE	TM	TE
efficiency	5.9451	6.2087	9.6186	13.4627	36.4519	29.1806	17.2408	14.4388	10.1308	8.3274	10.827	8.3194	8.3482	6.3055	8.3304	7.8097	6.7118	5.6534
intensity	6.4	3.7	10.58	7	50	19.5	14	5.7	8.8	3.5	7.7	3	5.4	1.95	4.25	1.95	2.7	1.3
intensity ratio	1.72972973		1.511428571		2.564102564		2.456140351		2.514285714		2.566666667		2.769230769		2.179487179		2.076923077	

Focus	13.3333		13.3333		13.3333		13.3333		13.3333		13.3333		13.3333		13.3333		13.3333	
lambda (lens)	1		1		1		1		1		1		1		1		1	
zones	11		11		11		11		11		11		11		11		11	
index	1.5		1.5		1.5		1.5		1.5		1.5		1.5		1.5		1.5	
lambda (1 = 450 nm)	0.6667		0.7778		0.8889		1		1.1111		1.2222		1.3333		1.4444		1.5556	
angle	90		90		90		90		90		90		90		90		90	
samp rate	20		20		20		20		20		20		20		20		20	
mode	TM	TE	TM	TE	TM	TE	TM	TE	TM	TE	TM	TE	TM	TE	TM	TE	TM	TE
efficiency	10.3524	4.3638	6.6981	8.6627	10.3907	9.5239	39.7132	35.9566	17.7547	12.3767	12.3896	10.2613	12.8637	9.9772	10.0723	8.295	7.2828	6.3121
intensity	14.5	2.8	5.8	4.5	10.2	5.7	49.5	20.25	13	4.45	8.1	3.5	8.4	3.2	4.8	1.95	3.5	1.55
intensity ratio	5.178571429		1.288888889		1.789473684		2.444444444		2.921348315		2.314285714		2.625		2.461538462		2.258064516	

Focus	13.3333		13.3333		13.3333		13.3333		13.3333		13.3333		13.3333		13.3333		13.3333	
lambda (lens)	1		1		1		1		1		1		1		1		1	
zones	11		11		11		11		11		11		11		11		11	
index	1.5		1.5		1.5		1.5		1.5		1.5		1.5		1.5		1.5	
lambda (1 = 450 nm)	0.6667		0.7778		0.8889		1		1.1111		1.2222		1.3333		1.4444		1.5556	
angle	80		80		80		80		80		80		80		80		80	
samp rate	20		20		20		20		20		20		20		20		20	
mode	TM	TE	TM	TE	TM	TE	TM	TE	TM	TE	TM	TE	TM	TE	TM	TE	TM	TE
efficiency	6.4654	7.7316	15.7851	9.93	15.6287	11.0334	20.6254	17.0989	22.4019	18.4678	18.9921	18.6011	8.6859	5.7969	7.6824	6.4465	6.8999	6.0736
intensity	13	5.7	16	5.5	16.2	5.6	20	7.9	18	7	13.9	5.9	5.8	1.95	3.8	1.58	3.7	1.62
intensity ratio	2.280701754		2.909090909		2.892857143		2.53164557		2.571428571		2.355932203		2.974358974		2.405063291		2.283950617	

APPENDIX C

Focus	12		12		12		12		12		12		12		12		12	
lambda (lens)	1		1		1		1		1		1		1		1		1	
zones	10		10		10		10		10		10		10		10		10	
index	1.5		1.5		1.5		1.5		1.5		1.5		1.5		1.5		1.5	
lambda (1 = 500 nm)	0.6		0.7		0.8		0.9		1		1.1		1.2		1.3		1.4	
angle	90		90		90		90		90		90		90		90		90	
samp rate	20		20		20		20		20		20		20		20		20	
mode	TM	TE	TM	TE	TM	TE	TM	TE	TM	TE	TM	TE	TM	TE	TM	TE	TM	TE
efficiency	11.9389	5.6006	9.9211	4.8903	7.3588	10.4514	14.954	10.9169	42.6296	36.4632	18.5433	13.8882	13.5576	11.2707	12.2295	13.0377	9.6103	8.429
intensity	18	4.1	13	4.2	7.1	5.4	15.8	5.6	50	20	11.6	4.2	7.3	2.9	6.8	3.5	4.85	2
intensity ratio	4.390243902		3.095238095		1.314814815		2.821428571		2.5		2.761904762		2.517241379		1.942857143		2.425	

Focus	10		10		10		10		10		10		10		10		10	
lambda (lens)	1		1		1		1		1		1		1		1		1	
zones	8		8		8		8		8		8		8		8		8	
index	1.5		1.5		1.5		1.5		1.5		1.5		1.5		1.5		1.5	
lambda (1 = 600 nm)	0.5		0.5833		0.667		0.75		0.8333		0.9167		1		1.0833		1.1667	
angle	90		90		90		90		90		90		90		90		90	
samp rate	20		20		20		20		20		20		20		20		20	
mode	TM	TE	TM	TE	TM	TE	TM	TE	TM	TE	TM	TE	TM	TE	TM	TE	TM	TE
efficiency	23.18	17.504	12.84	5.8243	10.6551	5.07	8.1531	9.67	9.8513	14.4	17.037	15.64	43.493	35.41	23.703	18.71	18.58	16.875
intensity	37.5	14.5	14.5	3.4	10	3.1	5.4	3.6	7	5.4	15.8	6.3	40	16	16.8	6.4	11.7	5.1
intensity ratio	2.586206897		4.264705882		3.225806452		1.5		1.296296296		2.507936508		2.5		2.625		2.294117647	

Focus	8.571		8.571		8.571		8.571		8.571		8.571		8.571		8.571		8.571	
lambda (lens)	1		1		1		1		1		1		1		1		1	
zones	6		6		6		6		6		6		6		6		6	
index	1.5		1.5		1.5		1.5		1.5		1.5		1.5		1.5		1.5	
lambda (1 = 700 nm)	0.4286		0.5		0.5714		0.6429		0.7143		0.7857		0.8571		0.9286		1	
angle	90		90		90		90		90		90		90		90		90	
samp rate	20		20		20		20		20		20		20		20		20	
mode	TM	TE	TM	TE	TM	TE	TM	TE	TM	TE	TM	TE	TM	TE	TM	TE	TM	TE
efficiency	14.4337	9.7723	21.2378	20.1763	22.8557	17.7278	17.5098	10.5018	12.2541	8.007	12.8399	14.0992	15.7469	12.8499	27.2457	20.5177	44.5887	31.5887
intensity	14.4	4.6	22.5	12.5	19	4.9	15	4.3	6.9	2.25	6.25	4.5	11.5	5.2	14.8	6	32	11
intensity ratio	3.130434783		1.8		3.87755102		3.488372093		3.066666667		1.388888889		2.211538462		2.466666667		2.909090909	